A new regional-scale multibeam echosounder bathymetric dataset of the Saudi Arabian Red Sea

Fabio Marchese[1], Marta Andrea Ezeta Watts[1,2], Megan Klein Breteler Nolan[1,2], Natalie Dunn[1,2], Katherine von Krusenstiern[3], Craig Foy[3], Mattie Rodrigue[3], Mohammed Qurban[4], Carlos Manuel Duarte[1,2], Vincent Pieribone[3], Francesca Benzoni[1,2]

[1] Division of Biological and Environmental Science and Engineering (BESE), King Abdullah University of Science and Technology (KAUST), Thuwal, 23955, Saudi Arabia
[2] Marine Science Program, Division of Biological and Environmental Science and Engineering (BESE), King Abdullah University of Science and Technology (KAUST), Thuwal, 23955, Saudi Arabia
[3] OceanX, New York, NY, 10018, United States
[4] National Center for Wildlife Development, Riyadh, 12411, Saudi Arabia

Correspondence to: Fabio Marchese (fabio.marchese@kaust.edu.sa)

Abstract. High-resolution bathymetry is a critical resource for marine research, underpinning seafloor characterisation, benthic habitat mapping, geomorphological analyses, and marine spatial planning. In the Red Sea, however, publicly accessible high-resolution bathymetric data remain extremely limited along the eastern margin. Existing regional products such as the General Bathymetric Chart of the Oceans (GEBCO) provide only coarse resolution coverage, and detailed surveys have historically been concentrated along the central axis rather than the Saudi Arabian shelf and slope. Here, we present a high-resolution bathymetric dataset acquired during the 2022 Red Sea Decade Expedition (RSDE) along the Saudi Arabian margin of the Red Sea (https://doi.org/10.5281/zenodo.19065211, Marchese et al., 2026). Multibeam echosounder surveys span approximately 860 km of coastline and extend from shallow coastal waters to deep-sea environments, covering depths from ~2 m >2,460 m. Data were acquired using multiple platforms and processed through a standardised workflow to produce a unified digital bathymetric model. Grid resolutions are 5 m for the shallow-water data and 40 m for the deep-water data, covering a total of 49,418.7 km² of seafloor. This dataset provides unprecedented spatial coverage of the eastern Red Sea seafloor and represents a key resource for marine sciences and marine spatial planning in a region where available detailed bathymetry has historically been limited.

1. Introduction

The Red Sea is a young, narrow ocean basin extending between the Arabian Peninsula and northeastern Africa, characterised by strong latitudinal gradients in bathymetry, geomorphology, and oceanographic conditions (Lazar et al., 2012). The origin and evolution of the Red Sea has long been a subject of debate, with classical models defining it as a transitional rift at the latest stages of continental rifting (Cochran and Martinez, 1988; Ehrhardt et al., 2005), and recent works showing that it is acting as a mature ocean basin active for the last 13 Ma (Augustin et al., 2021). In contrast, the northernmost sector, the Gulf of Aqaba, is dominated by narrow shelves and steep slopes associated with the tectonics of the Dead Sea Transform Fault System (Ben-Avraham, 1985; Ben-Avraham et al., 1979; Ribot et al., 2021a; Weinstein et al., 2021). The seafloor morphology is further shaped by the movement of thick Miocene evaporite sequences (Feldens and Mitchell, 2015; Mitchell and Park, 2014), which overprint the basement structure and influence the distribution of modern carbonate buildups along the margins (Rowlands et al., 2014).

High-resolution bathymetric data are a critical prerequisite for understanding seafloor structure, benthic habitat distribution, and geohazard processes, and supporting offshore infrastructure development and marine management (Cogan et al., 2009). In the Red Sea, however, the availability of publicly accessible, high-resolution bathymetry has remained extremely limited. Existing regional products, such as the General Bathymetric Chart of the Oceans (GEBCO), provide only coarse resolution coverage (15 arcsec, ~450 m) that is insufficient to resolve seafloor morphology at the scales required for ecological or geomorphological studies. Available data from detailed multibeam surveys are concentrated along the central axis of the basin, associated with mid-ocean ridge investigations (Augustin et al., 2016b; Fittipaldi et al., 2025a, b; Schmidt et al., 2013) or the Gulf of Aqaba (Ribot et al., 2021a, b), whereas the Saudi Arabian shelf and slope remain largely unmapped at high resolution with the exception of the data from the recent M193 cruise (Lüdmann et al., 2023). This regional gap mirrors a global one.

Global mapping initiatives such as the Nippon Foundation–GEBCO Seabed 2030 Project (Mayer et al., 2018) aim to produce a complete map of the world ocean floor by 2030, and they depend on the integration of regional and local high-resolution surveys to progressively replace coarse grids. In recent years, comparable regional-scale, high-resolution MBES datasets have been released and made openly available for other basins, including the Tyrrhenian Sea (Foglini et al., 2025) and the Baltic Sea (Janowski et al., 2024, 2025). The dataset presented here extends this effort to the Saudi Arabian continental margin and slope, providing insights into these structurally complex and ecologically significant settings, which have until now lacked detailed bathymetric characterisation and remained absent from openly accessible high-resolution products.

The Red Sea Decade Expedition (RSDE), conducted from February to June 2022, was a multidisciplinary oceanographic campaign with primary scientific objectives focused on biological, ecological, and biogeochemical investigations, including the collection of sediment cores, environmental DNA (eDNA), and direct observations using crewed submersibles and remotely operated vehicles (ROVs) (Angulo-Preckler et al., 2023, 2024; Anker et al., 2023; Frappi et al., 2023; Frühe et al., 2025; Klein et al., 2025; Lim et al., 2025a, b; Macrina et al., 2025; Martynova et al., 2024; Nolan et al., 2025; Vicario et al., 2024; Vimercati et al., 2024a, b). In the expedition context, seafloor mapping was a foundational activity designed to support and contextualise sampling efforts. Survey operations were organised into four along-coast Legs, each subdivided into operational Phases targeting different depth ranges and environments. Bathymetric data acquisition was tightly coupled to the spatial and temporal requirements of other mission objectives, and therefore multibeam coverage was prioritised around dive sites, sampling transects, and areas of specific scientific interest rather than following a uniform grid strategy. This operational design resulted in a spatially heterogeneous bathymetric dataset, with variable coverage density and resolution across Legs and Phases. The bathymetric dataset described here represents the integrated outcome of these mission-driven surveys.

2. Data acquisition

2.1. Survey design and acquisition strategy

Bathymetric data were acquired during the Red Sea Decade Expedition (RSDE) from February to June 2022 aboard the R/V OceanXplorer (Fig. 1), with additional shallow-water coverage collected using the support vessel Metalshark38. The Multibeam echosounder system (MBES) survey was conducted opportunistically, primarily during night operations and while transiting between sites. As the expedition's primary objectives focused on sediment sampling, biological surveys, and environmental characterisation using ROV and crewed submersible dives, MBES surveys were designed to provide local- to regional-scale seafloor context to inform dive planning and sampling locations. Accordingly, survey line placement, orientation, and spacing were adjusted dynamically to accommodate operational priorities, dive schedules, and environmental conditions. This mission-driven acquisition strategy produced spatially heterogeneous bathymetric coverage, with higher-density mapping concentrated around high-activity dive and sampling areas and comparatively limited coverage in other regions (Fig. 1).

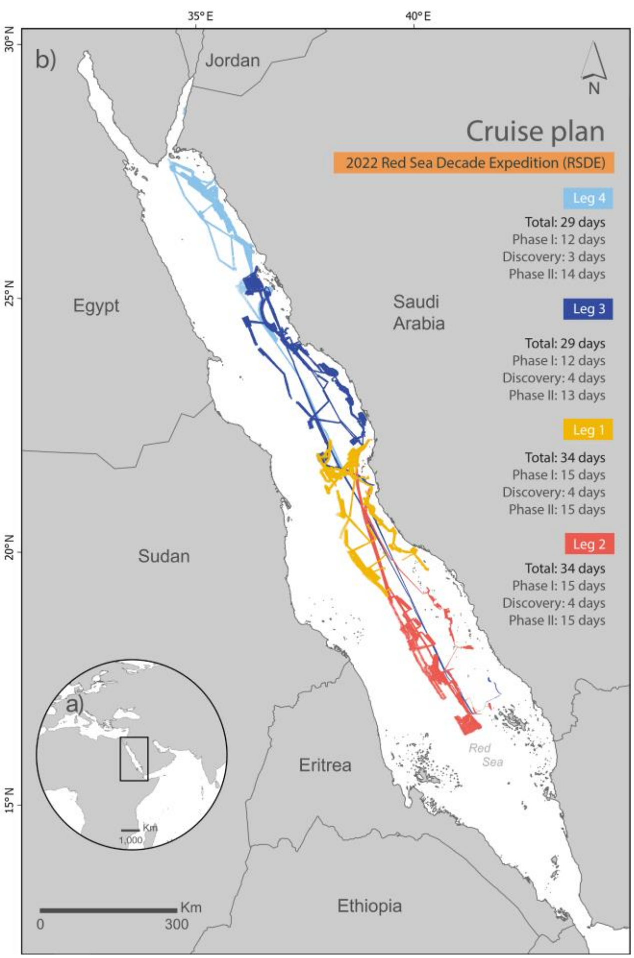

Figure 1: Cruise plan and spatial extent of bathymetric mapping during the 2022 Red Sea Decade Expedition (RSDE). Multibeam echosounder (MBES) survey areas acquired from the R/V OceanXplorer are shown across the Red Sea and coloured by expedition leg: Leg 1 (yellow), Leg 2 (red), Leg 3 (blue), and Leg 4 (light blue). Survey effort spanned the basin from the southern Red Sea to the northern Red Sea and the Gulf of Aqaba. For each Leg, the planned time allocation is shown in days. Coastlines from the GSHHG database (Wessel and Smith, 1996).

2.2. Survey instrumentation and sound-velocity correction

Deep-water bathymetry was acquired using a hull-mounted Kongsberg EM 304 multibeam echosounder (20–32 kHz) installed on the R/V OceanXplorer. Shallow-water bathymetry (generally < ∼100 m) was collected using a Teledyne RESON SeaBat T50-P multibeam echosounder (190–420 kHz) mounted on Metalshark38, a 38 ft support vessel deployed from the main ship (Fig. 2a). For both platforms, vessel positioning and attitude were provided by integrated GNSS and motion reference systems. Sound-velocity profiles used for multibeam correction were collected from 115 expendable bathythermograph (XBT) deployments conducted throughout the expedition. Profiles were collected opportunistically along survey lines to capture spatial and temporal variability in water-column structure, then stored and processed in Sound Speed Manager (Masetti et al., 2020) before being imported into Qimera during bathymetric processing.

3. Data processing

3.1. Processing workflow

MBES data were processed post-expedition at Habitat and Benthic Biodiversity Laboratory (HaBB), King Abdullah University of Science and Technology (KAUST) using Qimera v2.4.1 (QPS, Netherlands). Raw MBES files from all survey platforms were processed with a standardised workflow to ensure internal consistency across Legs, Phases, and acquisition systems, and to generate bathymetric surfaces suitable for regional- to local-scale analyses (Fig. 2).

Given the overall volume of the dataset and the spatial extent of the survey, MBES processing was distributed across multiple operators. Four dedicated processors independently handled the data from individual survey Legs for both the OceanXplorer deep-water acquisition and the Metalshark38 shallow-water surveys. A fifth processor coordinated the overall workflow, integrating and quality-checking the individual projects to ensure consistency across the full dataset.

This distributed processing strategy was implemented using the project-import functionality of Qimera, which allows projects to be exchanged as QPD files. Individual processors worked on separate project instances while periodically exporting updated QPD files that were imported into a central merged project. This configuration enabled near-real-time oversight of processing progress, cross-checking of cleaning decisions, and harmonisation of processing parameters across all Legs.

Sound-velocity corrections were applied using profiles processed with Sound Speed Manager (SSM), and navigation and altitude data were imported and verified. Tide corrections were applied using Red Sea tide stations available from the General Authority for Survey and Geospatial Information of Saudi Arabia (GASGI) database. Survey lines were then systematically inspected for timing offsets, navigation artefacts, and other acquisition issues prior to cleaning. Processing steps, including sound-velocity correction, manual and automated filtering, and adaptive cleaning based on depth and slope, were applied to minimise artefacts commonly associated with MBES data, such as outer-beam noise and slope-related distortions.

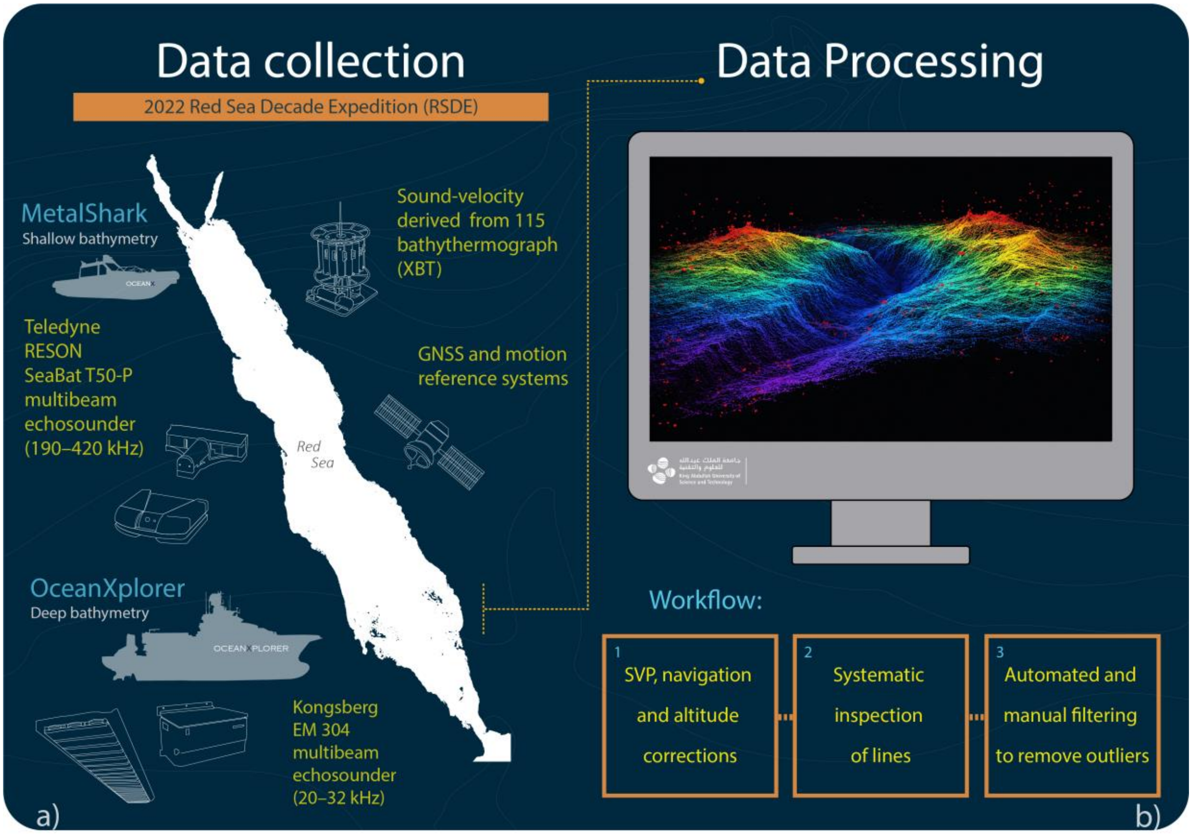

Figure 2: Survey instrumentation and bathymetry processing workflow. Panel a, Data collection. Deep- and intermediate-water bathymetry was acquired from the R/V OceanXplorer using a hull-mounted Kongsberg EM 304 multibeam echosounder (20–32 kHz). Shallow-water bathymetry was acquired from the support vessel Metalshark38 using a Teledyne RESON SeaBat T50-P multibeam echosounder (190–420 kHz). Vessel positioning and attitude were provided by integrated GNSS and motion reference systems. Sound-velocity information for multibeam correction was derived from 115 expendable bathythermograph (XBT) deployments collected throughout the expedition. Panel b, Data processing. MBES data were processed in Qimera following a standardised workflow comprising (1) sound-velocity, navigation, and altitude corrections, (2) systematic inspection and cleaning of survey lines, and (3) automated and manual filtering to remove outliers, producing the final corrected bathymetric surfaces.

3.2. System calibration

Prior to data acquisition, patch tests were performed for MBES systems to determine the angular mounting offsets of the transducer arrays relative to the vessel reference frame. The resulting roll, pitch, and heading offsets, as well as time latency values, were applied to all raw data during processing and are stored in the respective vessel configuration files in QPS Qimera. Table 1 summarises the calibration offsets for each system.

Table 1: Patch test calibration offsets applied during MBES data processing for the Kongsberg EM 304 (transmitter and receiver arrays) and Teledyne RESON SeaBat T50-P systems.

MBES system	Roll (°)	Pitch (°)	Heading (°)	Latency (s)
EM 304 Tx	0.12	0.48	0.04	0
EM 304 Rx	-0.11	0.87	0.04	0
RESON T50-P Tx	-1.40	2.52	0.1	0
RESON T50-P Rx	-1.40	2.52	0.1	0

3.3. Gridding and spatial coverage

After filtering processes, the accepted soundings were gridded into seven Digital Bathymetric Models (DBMs). Two fixed grid resolutions were applied: 5 m for shallow-water data acquired by the T50-P aboard Metalshark38, and 40 m for deep-water data acquired by the EM 304 aboard the R/V OceanXplorer, reflecting differences in depth, survey design, and line spacing among Legs and Phases (Table 2). Across the 2022 RSDE survey, a total of 2,863 MBES survey lines were processed, producing bathymetric coverage of 49,418.7 km² (Table 2). High-resolution shallow-water mapping collected from Metalshark38 contributed 133.8 km² of gridded bathymetry, while deep-water mapping from the R/V OceanXplorer contributed 49,284.9 km². Figure 3 shows the full extent of the gridded bathymetry across the Red Sea (panel a), which integrates all seven DBMs, alongside eight representative subsets (panels b–i), two per expedition Leg. These enlarged panels highlight the diversity of geomorphological settings captured by the survey. Erosive and gravity-driven processes are widespread along the margin, from gully fields incising the upper slope (panel b) to canyon flanks affected by slope instability (panel d) and a mass-wasting deposit related to a submarine landslide (panel g). Salt-related morphologies record the mobility of the widespread Miocene evaporites, expressed as a salt-flow lobate front (panel c) and as compressional ridges and flow lineaments related to salt movement (panel f) (Feldens and Mitchell, 2015; Mitchell et al., 2010). Volcanic and tectonic features characterise the deep central axis, including volcanic edifices and extensional lineaments (panel h) (Augustin et al., 2016a) and hummocky deposits related to lava flows in the Mabahiss Deep (panel e) (Fittipaldi et al., 2025b). Finally, panel i shows a pockmark field formed by fluids expelled through the underlying evaporite sequence (Feldens et al., 2016).

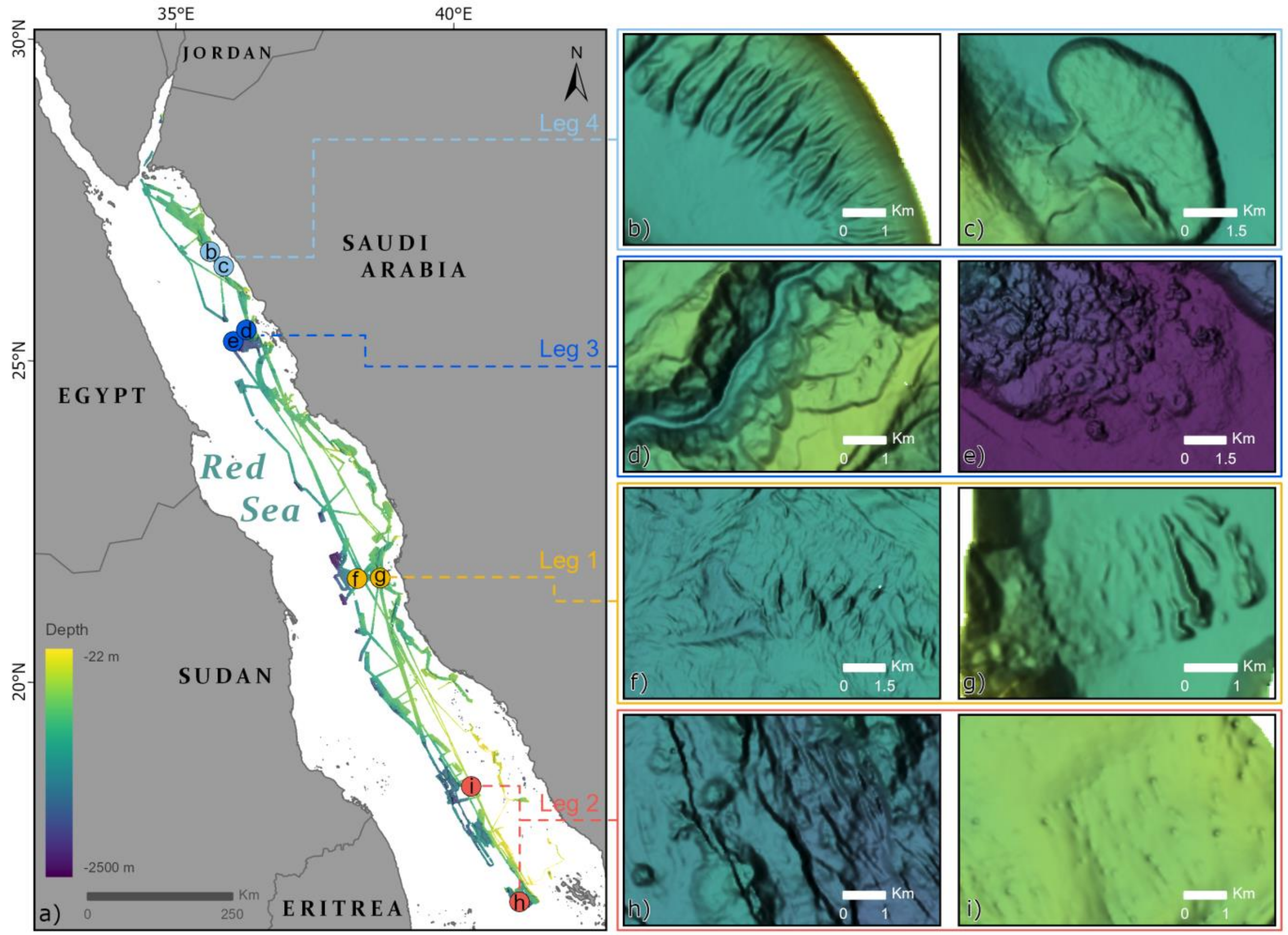

Figure 3: Final digital bathymetric models (DBMs) generated from RSDE multibeam surveys. Panel a, overview map integrating all seven DBMs, coloured by depth (metres). Panels b–i show representative examples of seafloor morphology, two per expedition Leg. Panel b, gully field on the upper slope (Leg 4). Panel c, salt-flow lobate front (Leg 4). Panel d, canyon flanks affected by slope instability (Leg 3). Panel e, hummocky deposits related to lava flows (Leg 3). Panel f, compressional ridges and flow lineaments related to salt movement (Leg 1). Panel g, mass-wasting deposit related to a submarine landslide (Leg 1). Panel h, volcanic cones and extensional lineaments along the central axis (Leg 2). Panel i, pockmark field (Leg 2). Scale bars in kilometres. Coastlines from the GSHHG database (Wessel and Smith, 1996).

Table 2: Summary of the Legs (L) and Phase (P): acquisition period, number of survey lines, resolution, area mapped. The survey effort was organized into four sequential geographic Legs (L1 to L4) conducted between February and June 2022. Operational Phases (P) represent subdivisions of each Leg targeting specific depth ranges and scientific objectives. Data acquisition was performed using two distinct platforms and multibeam echosounder (MBES) systems: the R/V OceanXplorer (OCX), equipped with a hull-mounted Kongsberg EM 304 for deep-water environments (40 m resolution), and the support vessel Metalshark38 (MS), equipped with a Teledyne RESON SeaBat T50-P for shallow-water targets (5 m resolution). The listed area coverage (km²) corresponds to the final gridded Digital Bathymetric Models (DBMs) available in the public repository. Note that the reported overall total area for EM304 represents the net unique seafloor area mapped (*). This value is lower than the arithmetic sum of individual leg and phase areas due to spatial overlaps occurring during transits and opportunistic re-surveys.

Leg and Phase	Date	MBES Survey lines (n)	DBM Resolution (m)	Area coverage (km²)
L1P1	02 - 2022	196	40	7,068.5
L1D	02 - 2022	40	40	1,089.6
L1P2	02/3 - 2022	196	20	3,834.2
L1P2-MS	02/03 - 2022	130	5	14.6
Total		562		12,006.9
L2P1	03 - 2022	218	40	9,377.6
L2P2	03/04 - 2022	222	25	4,740.5
L2P2-MS	03/04 - 2022	213	5	42.2
Total		653		14,160.2
L3D	04 - 2022	183	40	6,854.3
L3P1	04/05 - 2022	127	40	5,050.7
L3P2	05 - 2022	336	30	6,145.6
L3P2-MS	05 - 2022	296	5	33.5
Total		942		18,084.1
L4P1	05/06 - 2022	143	30	6,297.7
L4P1-MS	05/06 - 2022	65	5	18.9
L4P2	06 - 2022	59	30	1,958.8
L4P2-MS	06 - 2022	107	5	24.5
L4D-MS	06 - 2022	207	5	45.7
L4D	06 - 2022	125	20	3,839.2
Total		706		12,184.8
T50P total		1,018	5	133.8
EM304 total *		1,845	40	49,284.9
Overall total *		2,863	5;40	**49,418.7**

4. Technical validation

The quality of the bathymetric dataset was assessed through internal consistency analysis with cross-check comparisons of overlapping soundings against reference grids, evaluated against the International Hydrographic Organization (IHO) Standards for Hydrographic Surveys, S-44 (6th Edition, 2024) (International Hydrographic Organization, 2024).

4.1. Internal consistency: cross-check analysis

In the absence of pre-existing processed bathymetric datasets in the surveyed areas, all cross-check analyses are self-consistency assessments in which the survey data are compared against reference grids derived from the same acquisition. Bathymetric studies in unmapped or poorly constrained areas commonly assess data quality through internal self-consistency metrics such as repeated surveys, overlapping swaths, and inter-pass disparity, rather than through comparison against independent grids (Calder and Mayer, 2003; Mohammadloo et al., 2020; Sauter et al., 2025).

Internal consistency of the processed bathymetric data were assessed using the cross-check tool in QPS Qimera, which computes the depth bias between individual soundings and a reference grid constructed from overlapping survey lines. Specifically, the analysis quantifies inter-pass disparity, defined as the vertical variability between overlapping soundings acquired during different survey passes or under different swath geometries (Sauter et al., 2025). By comparing these internal repetitions, the dispersion of the data is used as a proxy for total measurement uncertainty, ensuring that the final DBMs maintain high spatial coherence even in the absence of independent ground-truth datasets. Cross-check analyses were performed in one representative sub-area per MBES for both the first and last legs of the campaign (Leg 1 and Leg 4), providing a systematic assessment of data quality at the beginning and end of the five-month expedition. Validation was restricted to areas where survey line geometry allowed robust statistical evaluation, specifically where parallel survey lines were intersected by perpendicular or near-perpendicular line. The use of cross-lines maximises the detectability of inter-pass disparity. The selected sub-areas encompass the range of depth intervals and acquisition conditions encountered during the campaign and provide a consistent basis for evaluating internal data quality and system stability.

For the deep-water EM 304 dataset, cross-checks were conducted in areas L1P1 (Leg 1, February 2022) and L4P1 (Leg 4, May–June 2022), covering depth ranges of 569–1,682 m and 617–1,280 m, respectively. Results were compared against the depth-uncertainty limits (THU and TVU) of the IHO S-44 Exclusive Order, used here as a stringent numerical benchmark rather than as an applicable survey order, since these limits are the tightest defined in the standard. For the shallow-water T50-P dataset, cross-checks were conducted in areas L1P2 (Leg 1, February 2022) and L4P2 (Leg 4, June 2022), covering depth ranges of 44–136 m and 32–186 m, respectively, and evaluated against IHO S-44 Order 1, applicable to coastal and shelf environments. For all datasets a consistent geometry of survey lines was selected for the cross-check, a set of parallel lines crossed by a perpendicular one. The comparison grid has the same resolution of the final processed bathymetry, 40 m for EM304 and 5 m for T50P.

In all four areas, the cross-check tests were accepted under the respective IHO standards (Table 3). For the EM 304 system, depth bias means were 0.055 m (L1P1) and 0.077 m (L4P1), indicating negligible and mutually consistent systematic offset across the full duration of the campaign. For the T50-P system, depth bias means were 0.000 m (L1P2) and -0.008 m (L4P2), with standard deviations of 0.337 m and 0.246 m, the lowest values across all four validation areas, consistent with the higher sounding density and finer grid resolution achievable in shallow water. The close agreement between Leg 1 and Leg 4 results for both systems, separated by approximately five months of continuous operations, demonstrates the stability of the system calibrations over time.

Table 3: Summary of IHO cross-check results for the three representative validation areas. All tests "accepted". Error limits are depth-dependent and computed by Qimera according to the respective IHO S-44 standard at the mean depth of each area.

Area	System	Depth range (m)	IHO order	Mean diff (m)	Std dev (m)	Mean+2σ (m)	Error limit (m)
L1P1 (Leg 1)	EM 304	569–1682	EO (6th)	0.055	1.649	3.353	6.180
L4P1 (Leg 4)	EM 304	617–1280	EO (6th)	0.077	1.781	3.639	6.845
L1P2 (Leg 1)	T50-P	44–136	Order 1	0.000	0.337	0.675	1.060
L4P2 (Leg 4)	T50-P	32–186	Order 1	−0.008	0.246	0.501	1.101

5. Usage notes

5.1. Coordinate reference system and vertical datum

All bathymetric grids are projected in WGS 84 / UTM Zone 37N (EPSG:32637). The vertical datum is the Lowest Astronomical Tide (LAT). Tidal corrections were applied using predicted tide heights from the Saudi Tide Tables 2022 (Volume I: Red Sea and Gulf of Aqaba), published by the General Authority for Survey and Geospatial Information of Saudi Arabia (GASGI), in which all tidal heights are referenced to LAT.

5.2. Known limitations

Coverage is spatially heterogeneous across the dataset, reflecting the mission-driven acquisition strategy of the expedition: survey lines were planned dynamically to support dive operations and sampling activities rather than to achieve uniform areal coverage. Higher sounding density is therefore concentrated around dive and sampling sites, while other regions have comparatively sparse or absent coverage. In addition, typical sources of uncertainty inherent to multibeam echosounder data should be considered when using this dataset. These include depth-dependent uncertainty scaling, associated with increasing beam footprint size and decreasing signal-to-noise ratio with depth, as well as reduced accuracy at outer swath angles. Furthermore, steep seafloor slopes may introduce local artefacts due to beam geometry and interpolation effects during gridding. The increase in standard deviation with depth observed in the cross-check analysis is consistent with these well-established characteristics of MBES systems.

6. Data availability

The bathymetric dataset acquired during the 2022 Red Sea Decade Expedition is available on Zenodo at https://doi.org/10.5281/zenodo.19065211 (Marchese et al., 2026). The repository contains the following GeoTIFF raster files: one grid file covering the full deep-water survey area (40 m resolution), acquired by the Kongsberg EM 304 aboard the R/V OceanXplorer (OCX_RSDE2022), and six grid files of shallow-water bathymetry (5 m resolution) acquired by the Teledyne RESON SeaBat T50-P aboard Metalshark38 (MS_RSDE2022), named by Leg and Phase (Table 2). Each file contains a bathymetric model representing gridded water depth in metres, referenced to the Lowest Astronomical Tide (LAT), projected in WGS 84 / UTM Zone 37N (EPSG:32637). Files conform to the GeoTIFF 1.1 standard and are readable by any GDAL-compatible software, including QGIS, ArcGIS, and Python (rasterio, GDAL). No proprietary software is required to access the data. In accordance with international standards for geospatial metadata, each GeoTIFF file is accompanied by a metadata record in XML format, compliant with the ISO 19115 standard.

7. Code availability

No custom code was developed or used in the acquisition, processing, or validation of the dataset described in this paper.

8. Conclusion

This study presents a comprehensive regional-scale, high-resolution multibeam echosounder bathymetric dataset covering the Saudi Arabian margin of the Red Sea, acquired during the 2022 Red Sea Decade Expedition. The dataset comprises 2,863 survey lines collected from two platforms and processed into Digital Bathymetric Models at 5 m and 40 m resolution, covering 49,418.7 km² from shallow coastal waters to depths exceeding 2,460 m. Data quality was assessed through standard calibration procedures and internal cross-check analyses evaluated against IHO S-44 standards, indicating consistent performance across both shallow- and deep-water datasets throughout the expedition. Compared to existing regional products, which are limited by coarse resolution and incomplete coverage, the dataset provides improved spatial resolution and coverage along the Saudi Arabian Red Sea.

This work helps bridge a major gap in the region and provides a foundation for applications such as seafloor mapping, benthic habitat studies, and geomorphological analyses, while supporting the interpretation and planning of future observations in the region. Beyond its regional relevance, this dataset contributes to global seafloor mapping efforts such as the Nippon Foundation–GEBCO Seabed 2030 Project (Mayer et al., 2018), adding openly accessible high-resolution bathymetry for a previously under-mapped sector of the world ocean.

Author contribution

F.M.: Conceptualization, Methodology, Data acquisition, Data processing, Formal analysis, Writing – original draft, Writing – review & editing. M.A.E.W.: Data processing, Writing – original draft, Writing – review & editing. M.K.B.N., N.D.: Data processing, Writing – review & editing. K.v.K., C.F.: Data acquisition, Writing – review & editing. M.R., V.P.: Expedition logistics and coordination, Writing – review & editing. M.Q., C.M.D.: Expedition logistics and coordination, Funding acquisition, Writing – review & editing. F.B.: Supervision, Funding acquisition, Writing – original draft, Writing – review & editing.

Competing interests

The authors declare that they have no conflict of interest.

Acknowledgements

We are grateful to the National Center for Wildlife (NCW, Saudi Arabia) for inviting us to participate in the expedition, and we acknowledge M. Qurban, C. M. Duarte, and J. E. Thompson for their coordination and support. We also extend our sincere appreciation to Amanda Bittinger and Jason Meyers for their support in multibeam data acquisition, the crews of the R/V OceanXplorer and the KAUST Coastal and Marine Resources core lab team for their essential logistical and operational assistance throughout the expedition. We acknowledge the General Authority for Survey and Geospatial Information (GASGI) and the National Geospatial Center of Saudi Arabia for the use of the tide table for the multibeam data vertical correction, GEOSA user agreement 2357. The authors used AI-assisted writing tools for language editing and text refinement. The scientific content, data interpretation, and conclusions remain entirely the authors' own.

Financial support

The 2022 Red Sea Decade Expedition (RSDE) was funded by the National Center for Wildlife (NCW, Kingdom of Saudi Arabia). The Qimera software license was provided by King Abdullah University of Science and Technology (KAUST) through baseline funding awarded to F. Benzoni. (BAS/1/1090-01-01).

References

Angulo-Preckler, C., Steckbauer, A., Armelles, I., Agustí, S., Rodrigue, M., Pieribone, V., Qurban, M., and Duarte, C. M.: First record of a live adult heteropod Firoloida desmarestia in the Red Sea, Front. Mar. Sci., 10, 1215195, https://doi.org/10.3389/fmars.2023.1215195, 2023.

Angulo-Preckler, C., Steckbauer, A., Lim, K. K., Hissmann, K., Pieribone, V., Qurban, M., and Duarte, C. M.: In situ observation on two 'elusive' rhodaliid siphonophores (Cnidaria; Hydrozoa; Siphonophora) from the Red Sea, including a potential new species within the genus Archangelopsis, Front. Mar. Sci., 11, 1338782, https://doi.org/10.3389/fmars.2024.1338782, 2024.

Anker, A., Vimercati, S., Barreca, F., Marchese, F., Chimienti, G., Terraneo, T. I., Rodrigue, M., Eweida, A. A., Qurban, M., Duarte, C. M., Pieribone, V., and Benzoni, F.: Mesophotic and Bathyal Palaemonid Shrimp Diversity of the Red Sea, with the Establishment of Two New Genera and Two New Species, Diversity, 15, 1028, https://doi.org/10.3390/d15101028, 2023.

Augustin, N., van der Zwan, F. M., Devey, C. W., Ligi, M., Kwasnitschka, T., Feldens, P., Bantan, R. A., and Basaham, A. S.: Geomorphology of the central Red Sea Rift: Determining spreading processes, Geomorphology, 274, 162–179, https://doi.org/10.1016/j.geomorph.2016.08.028, 2016a.

Augustin, N., Feldens, P., Kwasnitschka, T., Schmidt, M., Al Farawati, R., and Basaham, A. S.: High resolution bathymetry of the Red Sea Rift (1 arc-second) from POSEIDON cruise POS408 and PELAGIA cruises 64PE350 and 64PE351, https://doi.org/10.1594/PANGAEA.860374, 2016b.

Augustin, N., van der Zwan, F. M., Devey, C. W., and Brandsdóttir, B.: 13 million years of seafloor spreading throughout the Red Sea Basin, Nat. Commun., 12, 2427, https://doi.org/10.1038/s41467-021-22586-2, 2021.

Ben-Avraham, Z.: Structural framework of the Gulf of Elat (Aqaba), northern Red Sea, J. Geophys. Res., 90, 703–726, https://doi.org/10.1029/JB090iB01p00703, 1985.

Ben-Avraham, Z., Almagor, G., and Garfunkel, Z.: Sediments and structure of the Gulf of Elat (Aqaba)-Northern Red Sea, Sediment. Geol., 23, 239–267, https://doi.org/10.1016/0037-0738(79)90016-2, 1979.

Calder, B. R. and Mayer, L. A.: Automatic processing of high-rate, high-density multibeam echosounder data, Geochem. Geophys. Geosyst., 4, 1048, https://doi.org/10.1029/2002GC000486, 2003.

Cochran, J. R. and Martinez, F.: Evidence from the northern Red Sea on the transition from continental to oceanic rifting, Tectonophysics, 153, 25–53, https://doi.org/10.1016/0040-1951(88)90006-6, 1988.

Cogan, C. B., Todd, B. J., Lawton, P., and Noji, T. T.: The role of marine habitat mapping in ecosystem-based management, ICES J. Mar. Sci., 66, 2033–2042, https://doi.org/10.1093/icesjms/fsp214, 2009.

Ehrhardt, A., Hübscher, C., and Gajewski, D.: Conrad Deep, Northern Red Sea: Development of an early stage ocean deep within the axial depression, Tectonophysics, 411, 19–40, https://doi.org/10.1016/j.tecto.2005.08.011, 2005.

Feldens, P. and Mitchell, N. C.: Salt flows in the Central Red Sea, in: The Red Sea: The Formation, Morphology, Oceanography and Environment of a Young Ocean Basin, edited by: Rasul, N. M. A. and Stewart, I. C. F., Springer, Berlin, Heidelberg, Germany, 205–218, https://doi.org/10.1007/978-3-662-45201-1_12, 2015.

Feldens, P., Schmidt, M., Mücke, I., Augustin, N., Al-Farawati, R., Orif, M., and Faber, E.: Expelled subsalt fluids form a pockmark field in the eastern Red Sea, Geo-Mar. Lett., 36, 339–352, https://doi.org/10.1007/s00367-016-0451-9, 2016.

Fittipaldi, M., Trippanera, D., Augustin, N., van der Zwan, F. M., Parisi, L., and Jonsson, S.: High resolution bathymetry of the Mabahiss Deep area, Northern Red Sea, https://doi.org/10.5281/zenodo.16928676, 2025a.

Fittipaldi, M., Trippanera, D., Augustin, N., van der Zwan, F. M., Parisi, L., and Jónsson, S.: Mabahiss Deep in the Northern Red Sea: New insights from high-resolution bathymetric mapping and analysis, Mar. Geol., 490, 107645, https://doi.org/10.1016/j.margeo.2025.107645, 2025b.

Foglini, F., Rovere, M., Tonielli, R., Castellan, G., Prampolini, M., Budillon, F., Cuffaro, M., Di Martino, G., Grande, V., Innangi, S., Loreto, M. F., Langone, L., Madricardo, F., Mercorella, A., Montagna, P., Palmiotto, C., Pellegrini, C., Petrizzo, A., Petracchini, L., Remia, A., Sacchi, M., Sanchez Galvez, D., Tassetti, A. N., and Trincardi, F.: A new multi-grid bathymetric dataset of the Gulf of Naples (Italy) from complementary multi-beam echo sounders, Earth Syst. Sci. Data, 17, 181–203, https://doi.org/10.5194/essd-17-181-2025, 2025.

Frappi, S., Williams, C., Pilcher, N., Rodrigue, M., Marshall, P., Pieribone, V., Qurban, M., and Duarte, C. M.: New depth records and novel feeding observations of three elasmobranchs species in the Eastern Red Sea, Front. Mar. Sci., 10, 1270257, https://doi.org/10.3389/fmars.2023.1270257, 2023.

Frühe, L., Klein, S. G., Angulo-Preckler, C., Martynova, A., Alamoudi, T., García, J. V. A., Arossa, S., Breavington, J., Frappi, S., Laiolo, E., Lim, K. K., Parry, A. J., Re, E., Rosas, D. E. R., Rodrigue, M., Steckbauer, A., Pieribone, V. A., Qurban, M. A., and Duarte, C. M.: Particle-associated bacterioplankton communities across the Red Sea, Environ. Microbiol., 27, e70075, https://doi.org/10.1111/1462-2920.70075, 2025.

International Hydrographic Organization: Standards for Hydrographic Surveys S-44 Edition 6.2.0, Monaco, 2024.

Janowski, Ł., Skarlatos, D., Agrafiotis, P., Tysiąc, P., Pydyn, A., Popek, M., Kotarba-Morley, A. M., Mandlburger, G., Gajewski, Ł., Kołakowski, M., Papadaki, A., and Gajewski, J.: High resolution optical and acoustic remote sensing datasets of the Puck Lagoon, Sci. Data, 11, 360, https://doi.org/10.1038/s41597-024-03199-y, 2024.

Janowski, Ł., Barańska, A., Bojke, A., Bona, R., Borecka, A., Cichowska, A., Dembska, G., Dombrowski, P., Dziaduch, D., Flasińska, A., Foit, S., Gadzińska, A., Gajewski, Ł., Gajewski, J., Galer-Tatarowicz, K., Ginał, K., Grzywińska, U., Górecka, I., Hruzdieva, O., Jurkiewicz-Gruszecka, E., Kaczmarek, N., Kalarus, M., Kamińska, M., Kałas, M., Korczak, S., Kołakowski, M., Kubacka, M., Kusio, T., Leszczyńska, E., Lisimenka, A., Marciniewicz-Mykieta, M., Michałek, M., Misiewicz, E., Nowak, J., Opioła, R., Pieckiel, P., Rogowska, K., Sontowski, M., Szafrańska, M., Szefler, K., Tarała, A., Wróblewski, R., Wysocki, P., and Załęski, K.: High-resolution hydroacoustic datasets for over 7000 km² of Southern Baltic, Earth Syst. Sci. Data, 17, 6839–6850, https://doi.org/10.5194/essd-17-6839-2025, 2025.

Klein, S. G., Frühe, L., Parry, A. J., Marchese, F., Nolan, M. K. B., Laiolo, E., Lim, K. K., Steckbauer, A., Breavington, J., Hempel, C. A., von Krusenstiern, K., van der Zwan, F. M., Re, E., Alamoudi, T., Alva Garcia, J. V., Arossa, S., Angulo-Preckler, C., Rodrigue, M., Pieribone, V. A., Qurban, M. A., Benzoni, F., and Duarte, C. M.: Deep oxygen-depleted depressions in a Red Sea coral reef sustain resistant ecosystems, PNAS Nexus, 4, pgaf049, https://doi.org/10.1093/pnasnexus/pgaf049, 2025.

Lazar, M., Ben-Avraham, Z., and Garfunkel, Z.: The Red Sea – New insights from recent geophysical studies and the connection to the Dead Sea fault, J. Afr. Earth Sci., 68, 96–110, https://doi.org/10.1016/j.jafrearsci.2012.04.001, 2012.

Lim, K. K., Angulo-Preckler, C., Hempel, C. A., Qurban, M. A., Pieribone, V. A., and Duarte, C. M.: Benthic feeding and diet partitioning in Red Sea mesopelagic fish resolved through DNA metabarcoding and ROV footage, Ecol. Evol., 15, e71091, https://doi.org/10.1002/ece3.71091, 2025a.

Lim, K. K., Angulo-Preckler, C., Rabaoui, L. J., Qurban, M. A., Pieribone, V. A., Duarte, C. M., and Uyeno, D.: Discovery of new species of mesoparasitic pennellid (Copepoda: Siphonostomatoida) from the endemic mesopelagic lightfish Vinciguerria mabahiss in the Red Sea, Parasite, 32, 43, https://doi.org/10.1051/parasite/2025038, 2025b.

Lüdmann, T., Westphal, H., Ariza-Fuentes, M., Castellan, G., Giovenzana, F., Kappelmann, Y., Marchese, F., Stuhr, M., Taviani, M., Vahrenkamp, V., Vicario, S., Vittori, V., and Party, M. S.: Red Sea Paleoenvironmental Evolution under Monsoon fluctuations in the Pleistocene to Holocene, Cruise No. M193, 08.09.2023 – 06.10.2023, Limassol (Cyprus) – Jeddah (Saudi Arabia), Bonn, 1–59, https://doi.org/10.48433/cr_m193, 2023.

Macrina, L., Terraneo, T. I., McFadden, C. S., Chimienti, G., Marchese, F., Vimercati, S., Vicario, S., Reimer, J. D., Purkis, S. J., Eweida, A. A., Pieribone, V., Qurban, M., Duarte, C. M., Rodrigue, M., van der Zwan, F. M., Augustin, N., Westphal, H., and Benzoni, F.: The hidden diversity of Saudi Arabian Red Sea octocorals revealed through a morpho-molecular assessment across bathymetric and latitudinal gradients, Sci. Rep., 15, 33651, https://doi.org/10.1038/s41598-025-17136-5, 2025.

Marchese, F., Nolan, M. K. B., Dunn, N., Ezeta Watts, M. A., von Krusenstiern, K., Foy, C., Rodrigue, M., Pieribone, V., Qurban, M. A., Duarte, C. M., and Benzoni, F.: The high-resolution bathymetric dataset of the Saudi Arabian Red Sea margin from the 2022 Red Sea Decade Expedition (Version 1.0), https://doi.org/10.5281/zenodo.19065211, 2026.

Martynova, A., Rodrigue, M., Pieribone, V., Qurban, M., and Duarte, C. M.: Density and distribution patterns of seafloor macrolitter in the eastern Red Sea, Sci. Total Environ., 953, 176042, https://doi.org/10.1016/j.scitotenv.2024.176042, 2024.

Masetti, G., Smith, M. J., Mayer, L. A., and Kelley, J. G. W.: Applications of the Gulf of Maine Operational Forecast System to enhance spatio-temporal oceanographic awareness for ocean mapping, Front. Mar. Sci., 6, 804, https://doi.org/10.3389/fmars.2019.00804, 2020.

Mayer, L., Jakobsson, M., Allen, G., Dorschel, B., Falconer, R., Ferrini, V., Lamarche, G., Snaith, H., and Weatherall, P.: The Nippon Foundation–GEBCO Seabed 2030 Project: The quest to see the world's oceans completely mapped by 2030, Geosciences, 8, 63, https://doi.org/10.3390/geosciences8020063, 2018.

Mitchell, N. C. and Park, Y.: Nature of crust in the central Red Sea, Tectonophysics, 628, 123–139, https://doi.org/10.1016/j.tecto.2014.04.029, 2014.

Mitchell, N. C., Ligi, M., Ferrante, V., Bonatti, E., and Rutter, E.: Submarine salt flows in the central Red Sea, Geol. Soc. Am. Bull., 122, 701–713, https://doi.org/10.1130/B26518.1, 2010.

Mohammadloo, T. H., Snellen, M., and Simons, D. G.: Assessing the performance of the multi-beam echo-sounder bathymetric uncertainty prediction model, Appl. Sci., 10, 4671, https://doi.org/10.3390/app10134671, 2020.

Nolan, M. K. B., Falkenberg, P., Marchese, F., Ezeta Watts, M. A., Dunn, N., Macrina, L., Nunes-Peinemann, V., Chimienti, G., Vimercati, S., Terraneo, T. I., Qurban, M., Pieribone, V., Duarte, C. M., and Benzoni, F.: Modelling the habitat distribution of the endemic azooxanthellate coral Madracis interjecta from the mesophotic to the deep Red Sea, Ecol. Evol., 15, e71456, https://doi.org/10.1002/ece3.71456, 2025.

Ribot, M., Klinger, Y., Jónsson, S., Avsar, U., Pons-Branchu, E., Matrau, R., and Mallon, F. L.: Active faults' geometry in the Gulf of Aqaba, southern Dead Sea fault, illuminated by multibeam bathymetric data, Tectonics, 40, e2020TC006443, https://doi.org/10.1029/2020TC006443, 2021a.

Ribot, M., Klinger, Y., Jónsson, S., Avsar, U., Pons-Branchu, E., Matrau, R., and Mallon, F. L.: Bathymetric data from the Gulf of Aqaba, https://doi.org/10.5281/zenodo.4607639, 2021b.

Rowlands, G., Purkis, S., and Bruckner, A.: Diversity in the geomorphology of shallow-water carbonate depositional systems in the Saudi Arabian Red Sea, Geomorphology, 222, 3–13, https://doi.org/10.1016/j.geomorph.2014.03.014, 2014.

Sauter, G., Fabbri, S. C., Frischknecht, C., Anselmetti, F. S., and Kremer, K.: A systemic approach to managing uncertainties in repetitive multibeam bathymetric surveys, Environ. Model. Softw., 186, 106333, https://doi.org/10.1016/j.envsoft.2025.106333, 2025.

Schmidt, M., Al-Farawati, R., Al-Aidaroos, A., and Kürten, B.: RV PELAGIA Fahrtbericht / Cruise Report 64PE350/64PE351 – JEDDAH-TRANSECT; 08.03. – 05.04.2012 Jeddah – Jeddah, 06.04 – 22.04.2012 Jeddah – Duba, GEOMAR Helmholtz-Zentrum für Ozeanforschung, 154 pp., https://doi.org/10.3289/GEOMAR_REP_NS_5_2013, 2013.

Vicario, S., Terraneo, T. I., Bocanegra Castano, C., Chimienti, G., Oury, N., Vimercati, S., Hume, B. C. C., Marchese, F., Nolan, M. K. B., Eweida, A. A., Purkis, S. J., Rodrigue, M., Pieribone, V., Qurban, M., Duarte, C. M., and Benzoni, F.: Lost in the dark: Antipatharia-Symbiodiniaceae association in the deep waters of the Red Sea, Front. Mar. Sci., 11, 1330118, https://doi.org/10.3389/fmars.2024.1330118, 2024.

Vimercati, S., Terraneo, T. I., Castano, C. B., Barreca, F., Hume, B. C. C., Marchese, F., Ouhssain, M., Steckbauer, A., Chimienti, G., Eweida, A. A., Voolstra, C. R., Rodrigue, M., Pieribone, V., Purkis, S. J., Qurban, M., Jones, B. H., Duarte, C. M., and Benzoni, F.: Consistent Symbiodiniaceae community assemblage in a mesophotic-specialist coral along the Saudi Arabian Red Sea, Front. Mar. Sci., 11, 1264175, https://doi.org/10.3389/fmars.2024.1264175, 2024a.

Vimercati, S., Terraneo, T. I., Marchese, F., Eweida, A. A., Rodrigue, M., Pieribone, V., Qurban, M., Duarte, C. M., and Benzoni, F.: Diversity and distribution of coral gall crabs associated with Red Sea mesophotic corals, Front. Mar. Sci., 11, 1305396, https://doi.org/10.3389/fmars.2024.1305396, 2024b.

Weinstein, D. K., Tamir, R., Kramer, N., Eyal, G., Berenshtein, I., Shaked, Y., Loya, Y., and Torfstein, A.: Mesophotic reef geomorphology categorization, habitat identification, and relationships with surface cover and terrace formation in the Gulf of Aqaba, Geomorphology, 379, 107548, https://doi.org/10.1016/j.geomorph.2020.107548, 2021.

Wessel, P. and Smith, W. H. F.: A global, self-consistent, hierarchical, high-resolution shoreline database, J. Geophys. Res., 101, 8741–8749, https://doi.org/10.1029/96JB00104, 1996.